


Article

Simple Thalidomide Analogs in Melanoma: Synthesis and Biological Activity

Alexia Barbarossa ^{1,†}, Alessia Catalano ^{1,†}, Jessica Ceramella ², Alessia Carocci ^{1,*}, Domenico Iacopetta ^{2,*}, Camillo Rosano ³, Carlo Franchini ^{1,†} and Maria Stefania Sinicropi ^{2,†}

¹ Department of Pharmacy-Drug Sciences, University of Bari "Aldo Moro", 70126 Bari, Italy; alexia.barbarossa@uniba.it (A.B.); alessia.catalano@uniba.it (A.C.); carlo.franchini@uniba.it (C.F.)

² Department of Pharmacy, Health and Nutritional Sciences, University of Calabria, Via Pietro Bucci, Arcavacata di Rende, 87036 Cosenza, Italy; jessicaceramella@gmail.com (J.C.); s.sinicropi@unical.it (M.S.S.)

³ Proteomics and Mass Spectrometry Unit, IRCCS Policlinico San Martino, L.go Rosanna Benzi 10, 16132 Genova, Italy; camillo.rosano@hsanmartino.it

* Correspondence: alessia.carocci@uniba.it (A.C.); domenico.iacopetta@unical.it (D.I.)

† These authors equally contributed to this work.

‡ Co-senior authors.

Abstract: Thalidomide is an old well-known drug that is still of clinical interest, despite its teratogenic activities, due to its antiangiogenic and immunomodulatory properties. Therefore, efforts to design safer and effective thalidomide analogs are continually ongoing. Research studies on thalidomide analogs have revealed that the phthalimide ring system is an essential pharmacophoric fragment; thus, many phthalimidic compounds have been synthesized and evaluated as anticancer drug candidates. In this study, a panel of selected in vitro assays, performed on a small series of phthalimide derivatives, allowed us to characterize compound **2k** as a good anticancer agent, acting on A2058 melanoma cell line, which causes cell death by apoptosis due to its capability to inhibit tubulin polymerization. The obtained data were confirmed by in silico assays. No cytotoxic effects on normal cells have been detected for this compound that proves to be a valid candidate for further investigations to achieve new insights on possible mechanism of action of this class of compounds as anticancer drugs.

Keywords: anticancer; apoptosis; drugs repositioning; molecular docking studies; thalidomide analogs; tubulin



Citation: Barbarossa, A.; Catalano, A.; Ceramella, J.; Carocci, A.; Iacopetta, D.; Rosano, C.; Franchini, C.; Sinicropi, M.S. Simple Thalidomide Analogs in Melanoma: Synthesis and Biological Activity. *Appl. Sci.* **2021**, *11*, 5823. <https://doi.org/10.3390/app11135823>

Received: 13 May 2021

Accepted: 21 June 2021

Published: 23 June 2021

Publisher's Note: MDPI stays neutral with regard to jurisdictional claims in published maps and institutional affiliations.



Copyright: © 2021 by the authors. Licensee MDPI, Basel, Switzerland. This article is an open access article distributed under the terms and conditions of the Creative Commons Attribution (CC BY) license (<https://creativecommons.org/licenses/by/4.0/>).

1. Introduction

Cancer is still a great health concern, as it is one of the main causes of death worldwide. A total of 19.3 million new cases of cancer were diagnosed last year, of which 10 million were fatal [1]. Among the different types of cancer, malignant melanoma is one of the most aggressive and deadly skin cancers, with an enormously increasing occurrence over the past few decades [2–4]. Melanoma is notoriously chemoresistant; nevertheless, chemotherapy represents the primary treatment for metastatic melanoma. Considering the major impact of chemotherapy in cancer management, and the problems related to chemotherapy that have not yet been solved, such as drug toxicity and resistance, particularly in the case of melanoma, research for newer and potent anticancer agents is of great significance. Over the past few years, numerous biologically active heterocyclic compounds have been synthesized and evaluated as anticancer drugs. Among these, many phthalimidic compounds have turned out to be antitumor drug candidates. The phthalimidic core represents the main pharmacophoric feature of thalidomide (Figure 1), a drug infamous for its teratogenic action, which, nevertheless, represents one of the most successful examples of drug repositioning in the treatment of cancer. Indeed, over the last few decades, the interest in this old drug has been renewed because of its efficacy in several

important disorders (such as multiple myeloma, breast cancer, and HIV-related diseases [5]) and its antiangiogenic and immunomodulatory properties. Several studies regarding the effects of thalidomide on metastatic melanoma have been reported. Since angiogenesis, and specifically the increased expression of vascular endothelial growth factor (VEGF), has been reported as an important step in disease progression, the use of thalidomide to enhance the antitumor activity of chemotherapy has been investigated in metastatic melanoma [6]. Furthermore, a number of literature data report the effect of thalidomide and its derivatives on tubulin polymerization, causing a perturbation of microtubule dynamics. Microtubules represent important biological targets in cancer treatment due to their involvement in crucial cellular functions [7,8]. It became clear that thalidomide exerts multifaceted properties; however, many aftereffects, such as deep vein thrombosis, peripheral neuropathy, constipation, somnolence, pyrexia, pain, and teratogenicity, have been reported, showing the need for careful and monitored use [9]. Thus, research efforts are directed toward the synthesis and optimization of new thalidomide analogs, mostly as new anticancer agents, lacking toxic effects and that are able to remove these limits and improve the pharmacological profile. [10,11]. As a part of an ongoing research program, directed toward the synthesis of several antitumor heterocyclic compounds [12–16], and our previous paper [17] concerning the antitumor activity of a thalidomide-correlated compound, we report herein the synthesis of a small series of phthalimide derivatives, obtained by directly connecting the N-terminus of the phthalimide moiety with a differently substituted aromatic ring (2a–l, Figure 1). These compounds have been investigated for their cytotoxic effects in a large panel of cancer cells, including two melanoma cell lines, namely A2058 derived from a metastatic site, and malignant melanoma cells Sk-Mel28, two breast cancer cell lines (triple negative MDA-MB-231 and ER(+) MCF-7) and a human cervix carcinoma HeLa cell line. The best cytotoxic activity was recovered for compound 2k on A2058 melanoma cell line. The ability of compound 2k to inhibit tubulin polymerization has also been reported and a molecular docking study supported the obtained results.

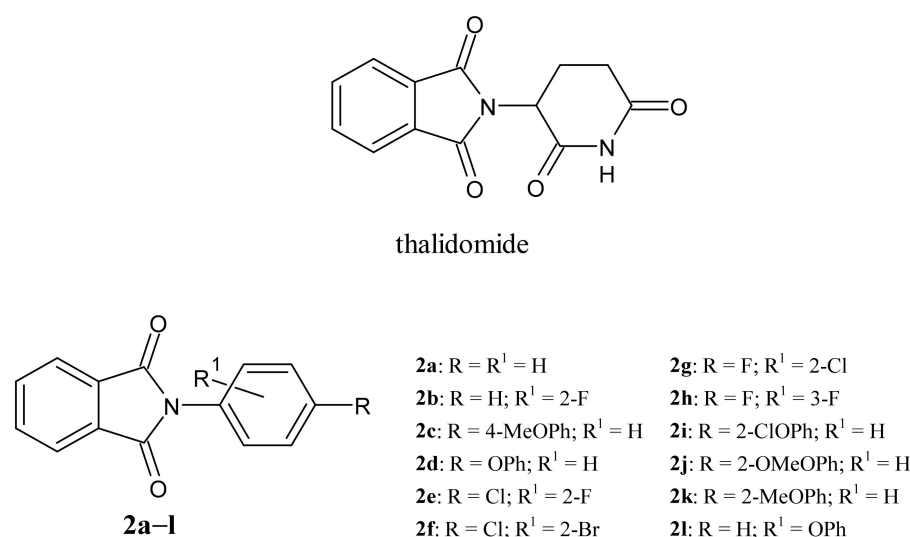


Figure 1. Structure of thalidomide and correlated compounds (2a–l).

2. Materials and Methods

2.1. Chemistry

All chemicals were supplied by Sigma-Aldrich or Alfa Aesar and were the highest-grade purity that were commercially available. Solvents were reagent grade unless otherwise indicated. Yields refer to purified products and were not optimized. Compound structures were confirmed by routine spectrometric analyses. Melting points were determined on a Gallenkamp melting point apparatus in open glass capillary tubes and are uncorrected. ¹H NMR and ¹³C NMR spectra were recorded on a Varian VX Mercury spec-

trometer operating at 300 and 75 MHz for ^1H and ^{13}C , respectively, or an Agilent 500 MHz operating at 500 and 125 MHz for ^1H and ^{13}C , respectively. Chemical shifts are reported in parts per million (ppm) relative to solvent (CDCl_3) resonance: δ 7.26 (^1H NMR) and δ 77.0 (^{13}C NMR). J values are given in Hz. The following abbreviations are used: s-singlet, d-doublet, t-triplet, and m-multiplet. Gas chromatography (GC)/mass spectroscopy (MS) was performed on a Hewlett-Packard 6890–5973 MSD at low resolution. Liquid chromatography (LC)/mass spectroscopy (MS) was performed on a spectrometer (Agilent 1100 series LC-MSD Trap System VL). Molecular ion was designed as “ M^+ ”. Elemental analyses were carried out on a Eurovector Euro EA 3000 analyzer and the data for C, H, N were within ± 0.4 of theoretical values.

Synthesis of 2-phenyl-1H-isoindol-1,3(2H)-dione (2a). Aniline (0.77 g, 8.3 mmol), phthalic anhydride (1.23 g, 8.3 mmol) and triethylamine (0.12 mL, 0.9 mmol) were refluxed in toluene (10 mL) for 5 h. The solvent was removed in vacuo and the residue, taken up with CHCl_3 , was washed 3 N HCl and water, and then dried over anhydrous Na_2SO_4 to give 905 mg (49%) of **2a** as a white solid: mp 211–213 °C; lit. 200 °C [18]; 210–211 °C (acetone) [19]. GC/MS (70 eV) m/z (%): 223 (M^+ , 100); LC/MS: m/z (%): 222 [$\text{M}^+ - 1$]; ^1H NMR (300 MHz, CDCl_3): δ 7.36–7.54 (m, 5H, Ar), 7.54–7.82 (m, 2H, Ar), 7.90–7.98 (m, 2H, Ar); ^{13}C NMR (75 MHz, CDCl_3): δ 123.7 (2C), 126.6 (1C), 128.1 (2C), 129.1 (2C), 131.8 (2C), 134.4 (2C), 167.3 (2C). Anal $\text{C}_{13}\text{H}_9\text{NO}_2$ (223.06): calcd %: C 75.33; H 4.06; N 6.27. Found %: C 74.98; H 4.04; N 6.30.

Synthesis of 2-(2-fluorophenyl)-1H-isoindol-1,3(2H)-dione (2b). Prepared as described for **2a** starting from 2-fluoroaniline. White solid. Yield: 65%: mp 190–191 °C (CHCl_3 /hexane); lit. 199 °C [19]; GC/MS (70 eV) m/z (%): 241 (M^+ , 92), 197 (100); ^1H NMR (500 MHz, CDCl_3): δ 7.23–7.30 (m, 2H, Ar), 7.35–7.38 (m, 1H, Ar), 7.42–7.47 (m, 1H, Ar), 7.79–7.82 (m, 2H, Ar), 7.95–7.98 (m, 2H, Ar); ^{13}C NMR (75 MHz, CDCl_3): δ 116.76 (d, $J = 19.6$ Hz, 1C), 119.4 (d, $J_{\text{CF}} = 13.7$ Hz, 1C), 123.9 (1C), 124.6 (d, $J_{\text{CF}} = 4.6$ Hz, 1C), 129.9 (2C), 130.7 (d, $J_{\text{CF}} = 8.0$ Hz, 1C), 131.9 (2C), 134.4 (2C), 157.9 (d, $J_{\text{CF}} = 251.9$ Hz, 1C), 166.5 (2C). Anal $\text{C}_{14}\text{H}_8\text{FNO}_2$ (241.05): calcd %: C 69.71; H 3.34; N 5.81. Found %: C 69.54; H 3.32; N 5.80.

Synthesis of 2-[4-(4-methylphenoxy)phenyl]-1H-isoindol-1,3(2H)-dione (2c). Prepared as described for **2a** starting from 4-*p*-tolylloxylaniline. Grey solid. Yield: 55%: mp 201–202 °C (CHCl_3 /hexane); GC/MS (70 eV) m/z (%): 329 (M^+ , 100); ^1H NMR (300 MHz, CDCl_3): δ 2.15–2.36 (m, 3H, CH_3), 6.97 (d, $J = 8.2$ Hz, 2H, Ar), 7.11 (d, $J = 21.7$ Hz, 2H, Ar), 7.16 (d, $J = 8.2$ Hz, 2H, Ar), 7.34 (d, $J = 8.8$ Hz, 2H, Ar), 7.76–7.79 (m, 2H, Ar), 7.92–7.95 (m, 2H, Ar); ^{13}C NMR (125 MHz, CDCl_3): δ 20.7 (1C), 118.3 (2C), 119.7 (2C), 123.7 (2C), 125.9 (1C), 128.0 (2C), 130.4 (2C), 131.8 (2C), 133.6 (1C), 134.4 (2C), 154.0 (1C), 157.8 (1C), 167.4 (2C). Anal $\text{C}_{21}\text{H}_{15}\text{NO}_3$ (329.11): calcd %: C 76.58; H 4.59; N 4.25. Found %: C 76.43; H 4.53; N 4.35.

Synthesis of 2-(4-phenoxyphenyl)-1H-isoindole-1,3(2H)-dione (2d). Prepared as described for **2a** starting from 4-phenoxyaniline. Grey solid. Yield: 65%: mp 161–162 °C (CHCl_3 /hexane); GC/MS (70 eV) m/z (%): 315 (M^+ , 100); ^1H NMR (500 MHz, CDCl_3): δ 7.06–7.15 (m, 5H, Ar), 7.35–7.38 (m, 4H, Ar), 7.78–7.79 (m, 2H, Ar), 7.94–7.95 (m, 2H, Ar); ^{13}C NMR (125 MHz, CDCl_3): δ 118.8 (2C), 119.5 (2C), 123.7 (2C), 123.9 (1C), 126.3 (1C), 128.0 (2C), 129.9 (2C), 131.7 (2C), 134.4 (2C), 156.5 (1C), 157.2 (1C), 167.4 (2C). Anal $\text{C}_{20}\text{H}_{13}\text{NO}_3 \cdot 0.20 \text{H}_2\text{O}$ (318.69): calcd %: C 75.32; H 4.23; N 4.39. Found %: C 75.60; H 4.08; N 4.48.

Synthesis of 2-(4-chloro-2-fluorophenyl)-1H-isoindol-1,3(2H)-dione (2e). Prepared as described for **2a** starting from 4-chloro-2-fluoroaniline. White solid. Yield: 35%: mp 145–146 °C; GC/MS (70 eV) m/z (%): 275 (M^+ , 100); ^1H NMR (500 MHz, CDCl_3): δ 7.25–7.32 (m, 3H, Ar), 7.78–7.82 (m, 2H, Ar), 7.90–7.98 (m, 2H, Ar); ^{13}C NMR (125 MHz, CDCl_3): δ 117.7 (d, $J_{\text{CF}} = 22.9$ Hz, 1C), 118.2 (d, $J_{\text{CF}} = 96.4$ Hz, 1C), 124.0 (2C), 125.1 (d, $J_{\text{CF}} = 3.8$ Hz, 1C), 130.5 (1C), 131.8 (2C), 134.6 (2C), 135.8 (d, $J_{\text{CF}} = 9.6$ Hz, 1C), 157.7 (d, $J_{\text{CF}} = 256.5$ Hz, 1C), 166.2 (2C). Anal $\text{C}_{14}\text{H}_7\text{ClFNO}_2 \cdot 0.25 \text{H}_2\text{O}$ (279.51): calcd %: C 60.02; H 2.70; N 5.00. Found %: C 60.42; H 2.50; N 5.07.

Synthesis of 2-(2-bromo-4-chlorophenyl)-1H-isoindol-1,3(2H)-dione (2f). Prepared as described for **2a** starting from 2-bromo-4-chloroaniline. White solid. Yield: 18%: mp 140–141 °C (CHCl_3 /hexane); GC/MS (70 eV) m/z (%): 337 (M^+ , 2), 302 (100); ^1H NMR (500 MHz,

CDCl₃): δ 7.24–7.30 (m, 1H, Ar), 7.45 (d, J = 8.8 Hz, 1H, Ar), 7.75 (s, 1H, Ar), 7.79–7.86 (m, 2H, Ar), 7.94–8.01 (m, 2H, Ar); ¹³C NMR (125 MHz, CDCl₃): δ 123.9 (1C), 124.0 (1C), 128.8 (2C), 130.1 (1C), 131.5 (1C), 131.8 (2C), 133.4 (1C), 134.6 (2C), 136.3 (1C), 166.3 (2C). Anal. C₁₄H₇BrClNO₂ (344.93): calcd %: C 49.96; H 2.10; N 4.16. Found %: C 49.96; H 2.05; N 4.15.

Synthesis of 2-(2-chloro-4-fluorophenyl)-1H-isoindol-1,3(2H)-dione (2g). Prepared as described for **2a** starting from 2-chloro-4-fluoroaniline. White solid. Yield: 68%: mp 188–189 °C (CHCl₃/hexane); GC/MS (70 eV) m/z (%): 275 (M⁺, 7), 240 (100); ¹H NMR (500 MHz, CDCl₃): δ 7.13 (t, J = 8.0 Hz, 1H, Ar), 7.32–7.35 (m, 2H, Ar), 7.80–7.84 (m, 2H, Ar), 7.94–8.00 (m, 2H, Ar); ¹³C NMR (125 MHz, CDCl₃): δ 115.1 (d, J_{CF} = 22.9 Hz, 1C), 117.9 (d, J_{CF} = 25.8 Hz, 1C), 124.0 (2C), 125.8 (d, J_{CF} = 3.9 Hz, 1C), 131.8 (d, J_{CF} = 8.7 Hz, 1C + s, 2C), 134.4 (d, J_{CF} = 11.4 Hz, 1C), 134.6 (2C), 162.7 (d, J_{CF} = 252.8 Hz, 1C), 166.6 (2C). Anal. C₁₄H₇ClFNO₂ (275.01): calcd %: C 61.00; H 2.56; N 5.08. Found %: C 60.71; H 2.49; N 5.06.

Synthesis of 2-(3,4-difluorophenyl)-1H-isoindol-1,3(2H)-dione (2h). Prepared as described for **2a** starting from 3,4-difluoroaniline. White solid. Yield: 52%: mp 199–200 °C; GC/MS (70 eV) m/z (%): 259 (M⁺, 100); ¹H NMR (300 MHz, CDCl₃): δ 7.22–7.39 (m, 3H, Ar), 7.78–7.84 (m, 2H, Ar), 7.93–7.99 (m, 2H, Ar); ¹³C NMR (75 MHz, CDCl₃): δ 116.0 (d, J_{CF} = 19.4 Hz, 1C), 117.5 (d, J = 18.6 Hz, 1C), 112.6 (d, J_{CF} = 4.6 Hz, 1C), 122.7 (d, J_{CF} = 3.4 Hz, 1C), 123.9 (2C), 127.9 (1C), 131.4 (2C), 134.6 (2C), 148.3 (dd, J_{CF} = 29.8, 12.6 Hz, 1C), 151.6 (dd, J = 28.0, 13.2 Hz, 1C), 166.8 (2C). Anal. C₁₄H₇FNO₂·0.20 H₂O (262.64): calcd %: C 63.98; H 2.84; N 5.33. Found %: C 64.32; H 2.69; N 5.38.

Synthesis of 2-[4-(2-chlorophenoxy)phenyl]-1H-isoindol-1,3(2H)-dione (2i). Prepared as described for **2a** starting from 4-(2-chlorophenoxy)aniline. Grey solid. Yield: 55%: mp 135–136 °C (CHCl₃/hexane); GC/MS (70 eV) m/z (%): 349 (M⁺, 100); ¹H NMR (500 MHz, CDCl₃): δ 7.11–7.15 (m, 4H, Ar), 7.24–7.28 (m, 1H, Ar), 7.37–7.40 (m, 2H, Ar), 7.47–7.48 (m, 1H, Ar), 7.78–7.80 (m, 2H, Ar), 7.93–7.96 (m, 2H, Ar); ¹³C NMR (125 MHz, CDCl₃): δ 117.9 (2C), 121.7 (1C), 123.8 (2C), 125.4 (1C), 126.4 (1C), 126.5 (1C), 128.0 (1C), 128.1 (1C), 130.9 (2C), 131.7 (2C), 134.4 (2C), 151.8 (1C), 156.7 (1C), 167.4 (2C). Anal. C₂₀H₁₂ClNO₃·0.50 H₂O (257.02): calcd %: C 66.95; H 3.65; N 3.90. Found %: C 67.32; H 3.36; N 4.02.

Synthesis of 2-[4-(2-methoxyphenoxy)phenyl]-1H-isoindol-1,3(2H)-dione (2j). Prepared as described for **2a** starting from 4-(2-methoxyphenoxy)aniline. Light brown solid. Yield: 75%: mp 148–150 °C (AcOEt/hexane). GC/MS (70 eV) m/z (%) 345 (M⁺, 100), 133 (100); ¹H NMR (300 MHz, CDCl₃): δ 3.84 (s, 3H, CH₃), 6.93–7.09 (m, 5H, Ar), 7.15–7.22 (m, 1H, Ar), 7.31–7.36 (m, 2H, Ar), 7.76–7.81 (m, 2H, Ar), 7.92–7.97 (m, 2H, Ar); ¹³C NMR (125 MHz, CDCl₃): δ 55.9 (1C), 113.0 (1C), 117.1 (2C), 121.1 (1C), 122.0 (1C), 123.7 (2C), 125.5 (1C), 125.6 (1C), 127.9 (2C), 131.8 (2C), 134.4 (2C), 144.0 (1C), 151.7 (1C), 157.9 (1C), 167.5 (2C). Anal. C₂₁H₁₅NO₄·H₂O (363.35): calcd %: C 69.63; H 4.91; N 3.54. Found: C 69.41; H 4.72; N 3.85.

Synthesis of 2-[4-(2-methylphenoxy)phenyl]-1H-isoindol-1,3(2H)-dione (2k). Prepared as described for **2a** starting from 4-(2-methylphenoxy)aniline. White solid. Yield: 33%: mp 123–124 °C (AcOEt/hexane); GC/MS (70 eV) m/z (%) 329 (M⁺, 100); ¹H NMR (500 MHz, CDCl₃): δ 2.25 (s, 3H, CH₃), 6.97–7.02 (m, 3H, Ar), 7.11 (t, J = 7.4 Hz, 1H, Ar), 7.21 (t, J = 7.4 Hz, 1H, Ar), 7.25–7.29 (m, 1H, Ar), 7.32–7.36 (m, 2H, Ar), 7.77–7.81 (m, 2H, Ar), 7.92–7.97 (m, 2H, Ar); ¹³C NMR (75 MHz, CDCl₃): δ 16.1 (1C), 117.3 (2C), 120.5 (1C), 123.7 (2C), 124.6 (1C), 125.6 (1C), 127.3 (1C), 127.9 (2C), 130.3 (1C), 131.6 (2C), 131.8 (2C), 134.3 (1C), 153.8 (1C), 157.7 (1C), 167.4 (2C). Anal. C₂₁H₁₅NO₃·0.50 H₂O (338.11): calcd %: C 74.79; H 4.96; N 4.45. Found: 74.54; H 4.77; N 4.14.

Synthesis of 2-(2-phenoxyphenyl)-1H-isoindol-1,3(2H)-dione (2l). Prepared as described for **2a** starting from 2-phenoxyaniline. Light pink solid. Yield: 70%: mp 146–148 °C; GC/MS (70 eV) m/z (%) 315 (M⁺, 100); ¹H NMR (300 MHz, CDCl₃): δ 6.96–7.10 (m, 4H, Ar), 7.18–7.31 (m, 3H, Ar), 7.33–7.42 (m, 2H, Ar), 7.71–7.79 (m, 2H, Ar), 7.87–7.95 (m, 2H, Ar). ¹³C NMR (125 MHz, CDCl₃): δ 119.0 (1C), 119.6 (2C), 122.4 (1C), 123.4 (1C), 123.7 (2C), 123.9 (1C), 129.7 (2C), 130.2 (1C), 130.5 (1C), 132.1 (2C), 134.1 (2C), 154.0 (1C), 156.3 (1C), 167.0 (2C). Anal. C₂₀H₁₃NO₃ (315.33): calcd %: C 76.06; H 4.20; N 4.43. Found: C 76.18; H 4.16; N 4.44.

2.2. Biological Methods

2.2.1. Cell Culture

The cell lines used in the present work (A2058, Sk-Mel28, MDA-MB-231, MCF-7, HeLa and HEK-293) were purchased from the American Type Culture Collection (ATCC, Manassas, VA, USA). All cell lines were maintained at 37 °C in a humidified atmosphere of 95% air and 5% CO₂ and periodically screened for contamination [20]. Human melanoma Sk-Mel-28 cells and human embryonic kidney HEK-293 cells, were cultured in Dulbecco's modified Eagle's medium (DMEM) high glucose (4.5 g/L) supplemented with 1% L-glutamine, 100 U/mL penicillin/streptomycin and 10% fetal bovine serum (FBS). The human melanoma cells A2058 were grown in DMEM low glucose (1 g/L) supplemented with 1% L-glutamine and 100 U/mL penicillin/streptomycin and 20% FBS. MCF-7 and MDA-MB-231 breast cancer cells were maintained in Dulbecco's modified Eagle's medium/nutrient mixture Ham F-12 (DMEM/F12), supplemented with 5% FBS and 100 U/mL penicillin/streptomycin. HeLa human epithelial cervix carcinoma cells were maintained in minimum essential Eagle's medium (MEM), supplemented with 10% FBS, 1% L-glutamine, 100 U/mL penicillin/streptomycin and 1% non-essential amino acids (NEAA).

2.2.2. MTT Assay

Cell viability was evaluated using the 3-(4,5-dimethylthiazol-2-yl)-2,5-diphenyltetrazolium (MTT, Sigma–Aldrich, Milan, Italy) assay as already reported [21]. Results are represented as percent (%) of basal and the IC₅₀ values were calculated using GraphPad Prism 9 (GraphPad Software, La Jolla, CA, USA).

2.2.3. Immunofluorescence Analysis

Cells were seeded in 48-well culture plates containing glass slides and incubated with the most active compound for 24 h (concentration equal to its IC₅₀ value), following a previously described protocol [22]. Rabbit anti β -tubulin was purchased from Santa Cruz Biotechnology and diluted to 1:100 before the use. The secondary antibody, Alexa Fluor[®] 568 conjugate goat-anti-mouse (1:500, Thermo Fisher Scientific, Waltham, MA, USA), was added and incubated for 2 h at 37 °C. Images were acquired using a fluorescence microscope (Leica DM 6000; 40 \times magnification). LAS-X software was used to process all images.

2.2.4. Tubulin Polymerization Assay

Tubulin polymerization inhibition was measured using an in vitro Tubulin Polymerization Assay Kit purchased from EMD Millipore Corporation [23], as already described [22]. The turbidity variation was measured every 30 s at 350 nm for 90 min, stirring the mixture for 10 s before each measurement.

2.2.5. TUNEL Assay

Apoptosis was detected using a TUNEL assay, according to the guidelines of the manufacturer (CFTM488A TUNEL Assay Apoptosis Detection Kit, Biotium, Hayward, CA, USA), as already reported [24]. Cells were observed and imaged under a fluorescence microscope (Leica DM6000; 20 \times magnification) with excitation/emission wavelength maxima of 490/515 nm (CF 488A) or 350/460 nm (DAPI). Images are representative of three independent experiments.

2.2.6. Western Blotting Analysis

Protein lysates were subjected to Western blot analysis, as already reported [25] Poly(ADP-ribose) polymerase 1 (Parp-1) and glyceraldehyde 3-phosphate dehydrogenase (GAPDH, used to verify the equal loading of proteins) were purchased from Santa Cruz Biotechnology (Santa Cruz, CA, USA). The antigen–antibody complex was detected by incubation of the membrane with a secondary antibody (peroxidase-coupled anti-rabbit

IgG, VWR International PBI, Milano, Italy). Immunoreactive bands were revealed using an ECL Western blotting detection system (Amersham Pharmacia Biotech, Piscataway, NJ, USA).

2.2.7. Docking Studies

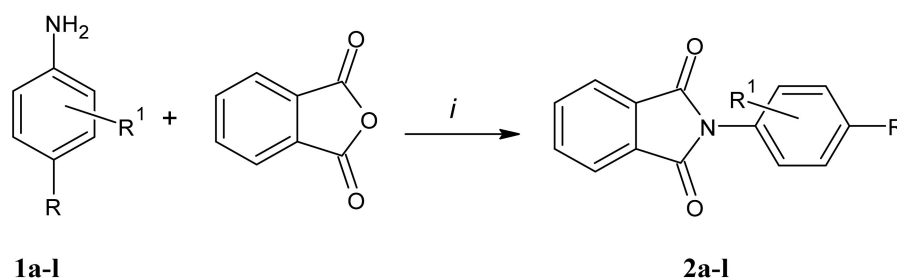
The crystal structure of the complex formed between a tetrameric assembly of tubulin and vinblastine [26]; PDB code 5j2t, was used as the protein target for our docking simulations. All the structures of the ligands tested in silico were designed, their 3D structures were created, charges were assigned and further energy was minimized using the program MarvinSketch (ChemAxon Ltd, Budapest, Hungary). To better characterize the binding mode and the mechanisms of action of the tested compounds to the protein target and to determine their binding energies, we used Autodock v.4.2.2. [27] and its graphical interface, ADT [28]. We performed all simulations using a searching grid with a cubic shape, composed of 126 points for each dimension, centered on the protein center. Nodes were spaced 0.375 Å from each other. Each of our simulation runs was performed adopting the default program values and the docking procedures were carried out as described in our previous works [20,29–32]. Briefly, the protein and the ligands were prepared using the ADT graphical interface by adding polar hydrogens to the protein and solvation parameters. During all the simulations, we considered the protein as a rigid object and the ligands as fully flexible. The Lamarckian genetic algorithm was used in our search with a population of 100 individuals that were evolved for 100 generations. The docking poses as resulting for our simulation runs were ranked in order of binding energy and collected into clusters on the basis of RMSD.

The generated docking poses were ranked in order of increasing binding energy values and clustered on the basis of a RMSD cut-off value of 2.0 Å. From the structural analyses of the lowest energy solutions of each cluster, we could identify the ligand binding mode. All the figures concerning the ligand binding modes to the protein target were drawn using the program Chimera [33].

3. Results and Discussion

3.1. Chemistry

The synthesis of the tested compounds was obtained by mixing equimolar quantities of phthalic anhydride and the suitable aryl amine in the presence of triethylamine (Scheme 1) [19].



Scheme 1. Synthesis of tested compounds. Reagents and conditions: (i) Et₃N, toluene, Δ, 5 h.

3.2. Biological Results

3.2.1. Cell Viability Assay

The cytotoxic activities of synthesized compounds (**2a-l**) were examined against two human melanoma cell lines, A2058, derived from a metastatic site, and malignant melanoma cells, Sk-Mel28, two breast cancer cells, ER(+) MCF-7 and triple negative MDA-MB-231 and the human epithelial cervix carcinoma HeLa cells. The calculated IC₅₀ values of studied compounds in comparison with the reference drug, thalidomide, are listed in Table 1. As shown, thalidomide did not exhibit any activity on both the cell lines at the higher concentration tested. None of the compounds were shown to possess anticancer

activity against the Sk-Mel28 cell line. Regarding the A2058 cell line, a slight activity was found for compound **2d**, which had no substituents on the phenoxy moiety. On the contrary, the presence of a chlorine substituent at the ortho position of the phenoxy nucleus seemed to enhance the activity since an IC_{50} of $23.26 \pm 1.1 \mu\text{M}$ was calculated for compound **2i** on A2058 cells. A notable inhibitory effect on the viability of the A2058 cell line, with an IC_{50} of $15.37 \pm 0.7 \mu\text{M}$, was obtained for compound **2k**, bearing a methyl group at the ortho position of the phenoxy moiety, which performed best out of the compound in the series. Similarly, compound **2k** exerted a good antitumor activity against both breast cancer cells used in this assay ($IC_{50} = 20.99 \pm 0.8$ and $22.72 \pm 0.9 \mu\text{M}$ on MDA-MB-231 and MCF-7, respectively), while no activity was recorded on HeLa cells. Compound **2i** was able to reduce the breast cancer cells growth with IC_{50} values amounting to 25.34 ± 1.0 and $31.2 \pm 1.2 \mu\text{M}$ on MDA-MB-231 and MCF-7 respectively, and, to a lesser extent, against cervix carcinoma HeLa cells growth ($IC_{50} = 54.5 \pm 0.8 \mu\text{M}$). A slight anticancer activity was also recovered for compound **2d** towards the breast cancer cells MDA-MB-231 ($IC_{50} = 76.5 \pm 1.2 \mu\text{M}$) and MCF-7 ($IC_{50} = 177.0 \pm 0.7 \mu\text{M}$) and towards HeLa cells ($IC_{50} = 42.1 \pm 1.1 \mu\text{M}$). No interesting activity was detected for the compounds lacking the phenoxy group against all cell lines used. To assess potential cytotoxicity towards normal cells, a screening of the compounds was performed on the non-tumoral human embryonic renal cell line Hek-293. As can be seen in Table 1, most of the compounds and thalidomide did not interfere with the normal cell viability, at least until the concentration of $200 \mu\text{M}$ and under the conditions used for this assay. A slight cytotoxicity was found for compound **2i**, though at a concentration 6-fold higher than the active one. A certain cytotoxicity against Hek-293 cell lines was found for compound **2c**, which, however, did not exhibit antitumor activity on the melanoma cells.

Table 1. IC_{50} values of compounds **2a–l** and thalidomide expressed in μM .

Compound	IC_{50} (μM)					
	A2058	Sk-Mel28	MDA-MB-231	MCF-7	HeLa	Hek-293
2a	>200	>200	>200	>200	>200	>200
2b	>200	>200	>200	>200	>200	>200
2c	>200	>200	>200	>200	>200	65.63 ± 0.8
2d	124.7 ± 0.9	>200	76.5 ± 1.2	177.0 ± 0.7	42.1 ± 1.1	>200
2e	>200	>200	>200	>200	>200	>200
2f	>200	>200	>200	>200	>200	>200
2g	>200	>200	>200	>200	>200	>200
2h	>200	>200	>200	>200	>200	>200
2i	23.26 ± 1.1	>200	25.34 ± 1.0	31.2 ± 1.2	54.5 ± 0.8	149.2 ± 0.9
2j	>200	>200	>200	>200	>200	>200
2k	15.37 ± 0.7	>200	20.99 ± 0.8	22.72 ± 0.9	>200	>200
2l	>200	>200	>200	>200	>200	>200
thalidomide	>200	>200	>200	>200	>200	>200

3.2.2. Effect of Compound **2k** on Microtubule Dynamics and Cell Death by Apoptosis

Microtubules represent vital cell components shaped by polymerization of α and β tubulin heterodimers and play crucial roles in several cellular functions, including cell division [34]. Several classes of naturally occurring, as well as synthetic and semi-synthetic, compounds disrupt microtubule organization, altering the tubulin dynamics. Among them, vinca alkaloids and taxanes are two families of microtubule-binding agents currently used for the treatment of different solid and hematological tumors, and are characterized by strong side effects [35]. Generally, microtubule-binding agents are divided into two main groups: microtubule-destabilizing and microtubule-stabilizing agents, able to suppress microtubule dynamics with different mechanisms. Particularly, microtubule-destabilizing agents, including vinca alkaloids, inhibit the tubulin polymerization and thus destabilize microtubules; instead, taxanes, including paclitaxel, bind to polymerized microtubules, stabilizing tubulin filaments [36]. Recently, agents able to regulate microtubule dynam-

ics, hampering tubulin polymerization or blocking microtubule disassembly, and free of adverse effects, have received great interest in anticancer therapy [37–39]. Given that our most active compound, **2k**, did not exert any cytotoxicity against the normal cells, we evaluated its ability to interfere with tubulin by using both an immunofluorescence assay and an in vitro tubulin-polymerization inhibition assay. Regarding the immunofluorescence assay, melanoma A2058 cells were exposed to compound **2k** or vinblastine, used as a reference molecule, for 24 h and then processed as described in the materials and methods. Figure 2 shows that, in the CTRL cells (vehicle-treated), tubulin resulted widely distributed in the cytoplasm, forming a regular arrangement and organization of the microtubules with normal and well-assembled filaments (Panel B, CTRL). On the contrary, A2058 cells exposed to vinblastine, as well as those treated with compound **2k**, revealed a dramatic disorganization of microtubules in which tubulin accumulated in the form of crystals within the cell cytoplasm (see white arrows, Figure 2, Panel B, vinblastine and **2k**). Thus, compound **2k** is able to perturb tubulin assembly, interfering with normal microtubule organization.

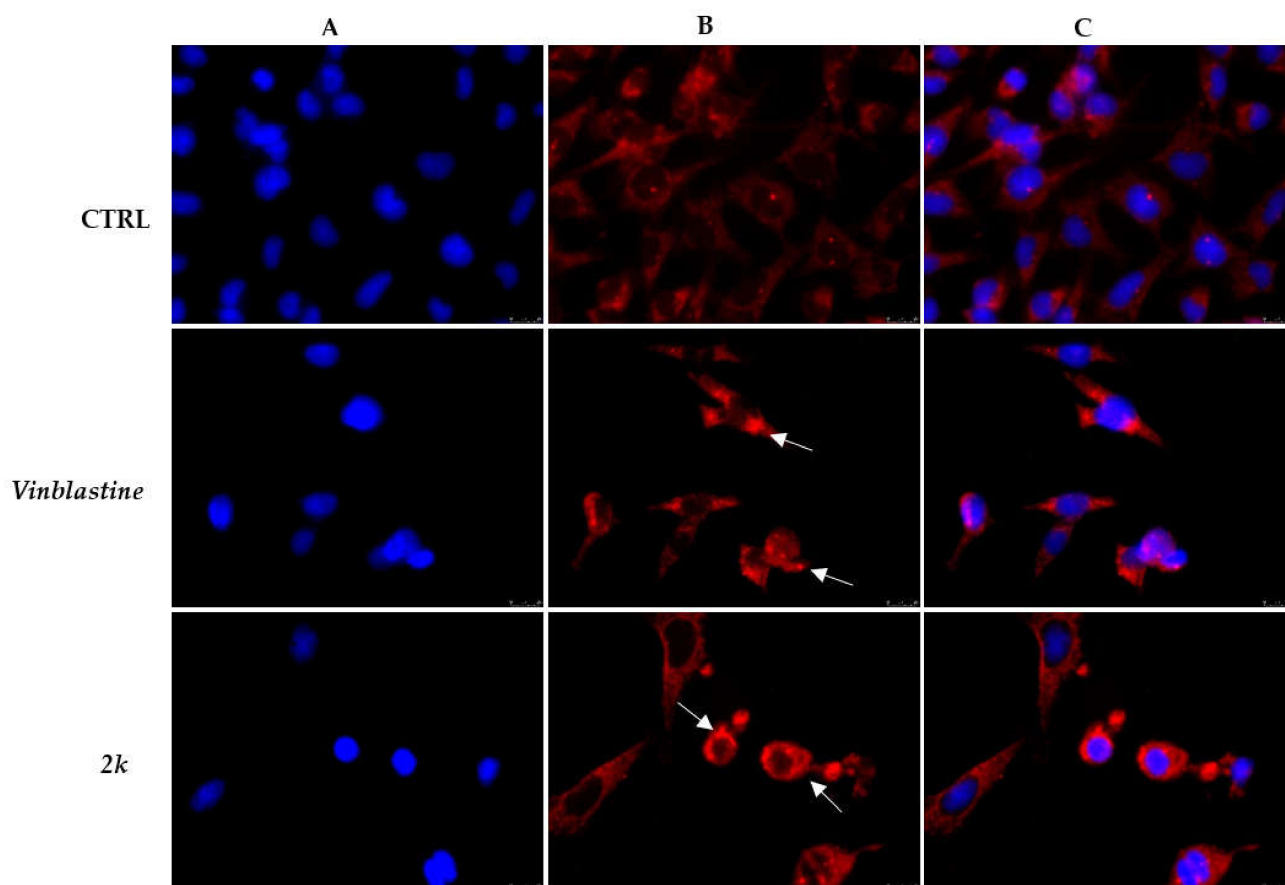


Figure 2. Immunofluorescence studies. Human melanoma A2058 cells were incubated with compound **2k**, with vinblastine (both used at their IC_{50} values), or with DMSO (CTRL) for 24 h. Cells were observed under the inverted fluorescence microscope at $40\times$ magnification. CTRL cells displayed a normal arrangement and organization of the tubulin cytoskeleton. Instead, A2058 cells treated with compound **2k** and vinblastine exhibited an irregular microtubules organization (see white arrows). (A) nuclear stain with DAPI ($\lambda_{ex} = 350\text{ nm}/\lambda_{em} = 460\text{ nm}$); (B) β -tubulin (Alexa Fluor[®] 568; $\lambda_{ex} = 644\text{ nm}/\lambda_{em} = 665\text{ nm}$); (C) overlay channel. Representative fields are shown.

Next, we evaluated if the detected microtubule disorder could be linked to the ability of compound **2k** to act as a destabilizing agent, inhibiting tubulin polymerization, or as a stabilizing agent. Thus, we performed an in vitro tubulin-polymerization inhibition assay, using paclitaxel and vinblastine as reference molecules, and compound **2k**, all used at a

concentration of 10 μM . In this assay, we measured the turbidity at 350 nm for 3600 s at 37 $^{\circ}\text{C}$ to evaluate the tubulin assembly. The obtained results, shown in Figure 3, demonstrated that, in the CTRL reaction, tubulin heterodimers polymerize in a time-dependent manner, reaching a plateau after about 15 min with a final optical density value at 350 nm (OD₃₅₀) of about 0.48. Instead, the exposure of tubulin to the microtubule-stabilizing agent, paclitaxel, caused an increase in tubulin polymerization, which reached a plateau after about 10 min with a final OD₃₅₀ higher than CTRL (OD₃₅₀ paclitaxel = 0.56). Contrarily, the microtubule-destabilizing agent vinblastine strongly blocked the tubulin polymerization and its curve reached the steady state only after 70 min with a very low final OD₃₅₀ (0.19). Similarly, the exposure of tubulin to the compound **2k** exerted an important inhibitory activity on the protein polymerization, even if in a lesser extent if compared with vinblastine. Indeed, the **2k** curve reaches the plateau in about 25 min with a turbidity value 1.5-fold less than the control reaction (OD₃₅₀ **2k** = 0.32). Taken together, these results suggest that compound **2k** perturbs microtubule dynamics due to its capability to inhibit tubulin polymerization.

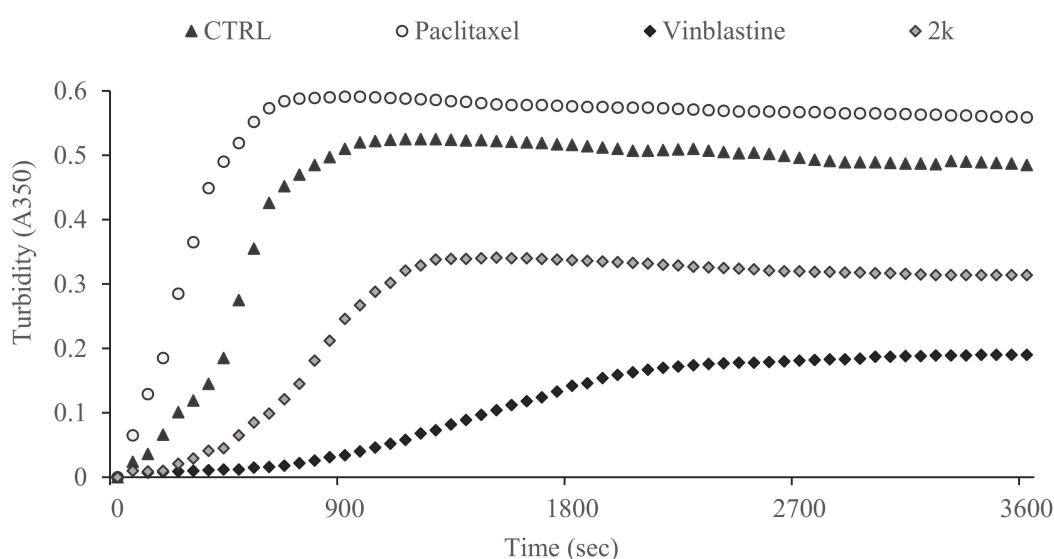


Figure 3. Tubulin polymerization assay. The *in vitro* tubulin polymerization was evaluated after tubulin incubation with compound **2k** used at the concentration of 10 μM . Vinblastine and paclitaxel (10 μM) were used as positive controls, while vehicle (DMSO) was used as a negative control. Tubulin polymerization was measured by determining the turbidity at 350 nm for 3600 s at 37 $^{\circ}\text{C}$.

Due to the great involvement of microtubules in cellular growth, they represent a good target for cancer treatment. Indeed, the disorganization of microtubules can be responsible of cell cycle arrest, subsequently triggering the programmed cell death of tumoral cells [22,23,40–42]. In order to investigate if compound **2k** induced apoptosis, we performed a TUNEL assay on A2058 cells, exposed for 24 h to this compound, used at its IC₅₀ value. The obtained results indicate that compound **2k** induced apoptosis in these cells. Indeed, in the treated cells is notable a clear green nuclear fluorescence due to the formation of fragmented DNA, substrate of the terminal deoxynucleotidyl transferase (TdT) enzyme (Figure 4, Panel B, compound **2k**). Contrarily, green fluorescence is totally absent in the nuclei of the CTRL cells (vehicle-treated cells), indicating no DNA breakage (Figure 4, Panel B, CTRL).

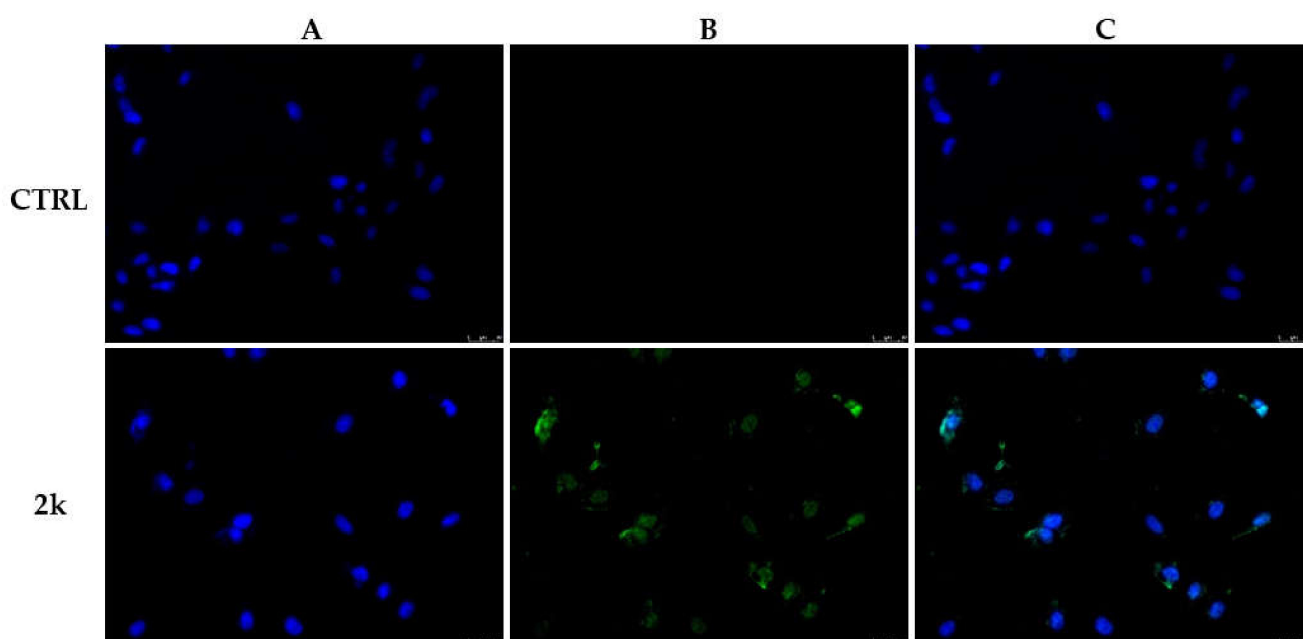


Figure 4. TUNEL assay. A2058 cells were treated with compound **2k** used at its IC_{50} value or with the vehicle (CTRL) for 24 h. Apoptotic death is clearly indicated by the green nuclear fluorescence, present in the A2058 cells treated with compound **2k** and absent in the CTRL cells. Images were acquired under an inverted fluorescence microscope at $20\times$ magnification. (A) DAPI (CTRL and compound **2k**) $\lambda_{ex} = 350\text{ nm}/\lambda_{em} = 460\text{ nm}$. (B) CFTM488A (CTRL and compound **2k**) $\lambda_{ex} = 490\text{ nm}/\lambda_{em} = 515\text{ nm}$. (C) Overlay channel. Fields are representative of three separate experiments.

The **2k**-induced apoptosis of melanoma A2058 cells was accompanied by Poly(ADP-ribose) polymerase-1 (PARP-1) cleavage. During the apoptosis process, cells exhibit several biochemical modifications, including the degradation of many proteins by caspases [43]. Among them, PARP-1 is converted from the 116-kDa form to a fragment of 89 kDa. PARP-1 is an eukaryotic protein that plays a vital role in DNA repair, replication, and differentiation, and is involved in the activation of cellular defense mechanisms against DNA damage [44]. During apoptotic death, caspases cause PARP-1 cleavage and inactivation, making it no longer able to repair DNA damage [45]. Thus, considering the importance of PARP-1 cleavage as a hallmark of apoptosis, we analyzed the status of this protein in A2058 cells treated with compound **2k** (used at its IC_{50} value) at different times (48 h and 72 h), performing a Western blot analysis. Treatment with compound **2k** induced proteolytic cleavage of PARP-1. Indeed, an accumulation of the 89-kDa cleavage fragment was observed (Figure 5, 48 h and 72 h) in a time dependent manner: the cleaved form of the protein was already visible 48 h after **2k** treatment and it gradually increased until 72 h. Contrarily, the native form of PARP-1 (116-kDa) decreased in a time-dependent manner in cells treated with compound **2k**, becoming hardly visible at 72 h. Instead, at time 0 h (Figure 5, 0 h), the uncleaved form is highly represented. Thus, these data indicate that apoptosis cell death induced by compound **2k** involves PARP-1 degradation.

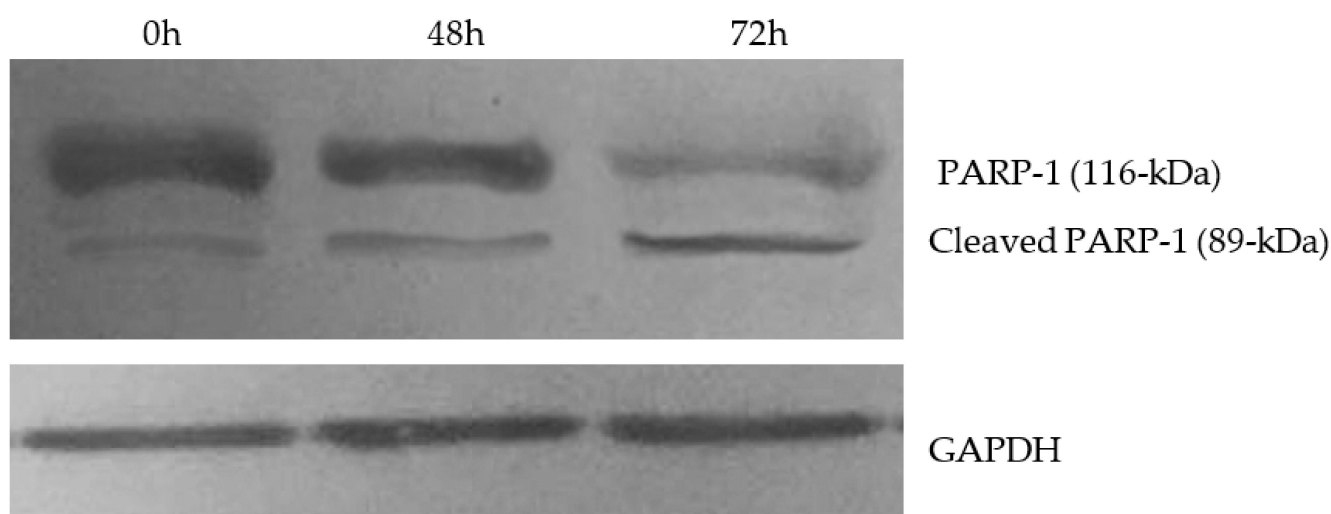


Figure 5. PARP-1 cleavage. A2058 melanoma were treated with compound **2k** (used at its IC_{50} value) for 48 and 72 h and then the total protein extracts were analyzed by Western blot. PARP-1 native form (116-kDa) and the cleaved form (89 kDa) were visualized. Time points 0 h, 48 h and 72 h for protein extraction. GAPDH was used for loading normalization. Blots are representative of three independent experiments.

3.2.3. Docking Studies

To first evaluate the binding poses and the calculated affinities between our more active compounds (**2d**, **2i** and **2k**) and tubulin and in order to screen the molecules for the best lead candidate, we performed molecular docking simulations using, as a target, the three-dimensional structure of tubulin in complex with its well-known ligand vinblastin, a vinca alkaloid that inhibits the formation of microtubules within cells [26]. Affinities of the three compounds to the protein were calculated using Autodock according to the expression $K_i = \exp(\Delta G / (R \cdot T))$. As discussed in our previous works [46–48], to identify the most promising compound, we adopted a strategy based on the clusterization of the results from our simulation runs, together with the visual inspection of the ligand-protein binding mode. All our compounds share the same protein binding site with vinblastine, at the interface between the β - and α -tubulin subunits (Figure 6) as determined by X-ray crystallography [26]. All the tested compounds seem to be good ligands of the protein. They are almost superimposed over each other and share most of the interactions with the protein amino acids. Particularly, molecule **2d** is positioned within the vinblastine binding site of tubulin, forming hydrogen bonds with protein residues Asp β 179 and Tyr β 224. This binding mode is stabilized by hydrophobic interactions with residues Tyr β 210, Phe β 214, Val β 217, Pro β 222, Ile α 332, and Phe α 351. Ligands **2k** and **2i** share the same interactions described above with **2d**, but form an additional hydrophobic interaction with Val α 328. The slightly different activity of **2i** in comparison with **2k** might be due to the hydrophobic environment surrounding the CH_3 group of **2k**, unlike the more hydrophilic chlorine atom present in ortho position of the phenoxy portion of **2i**.

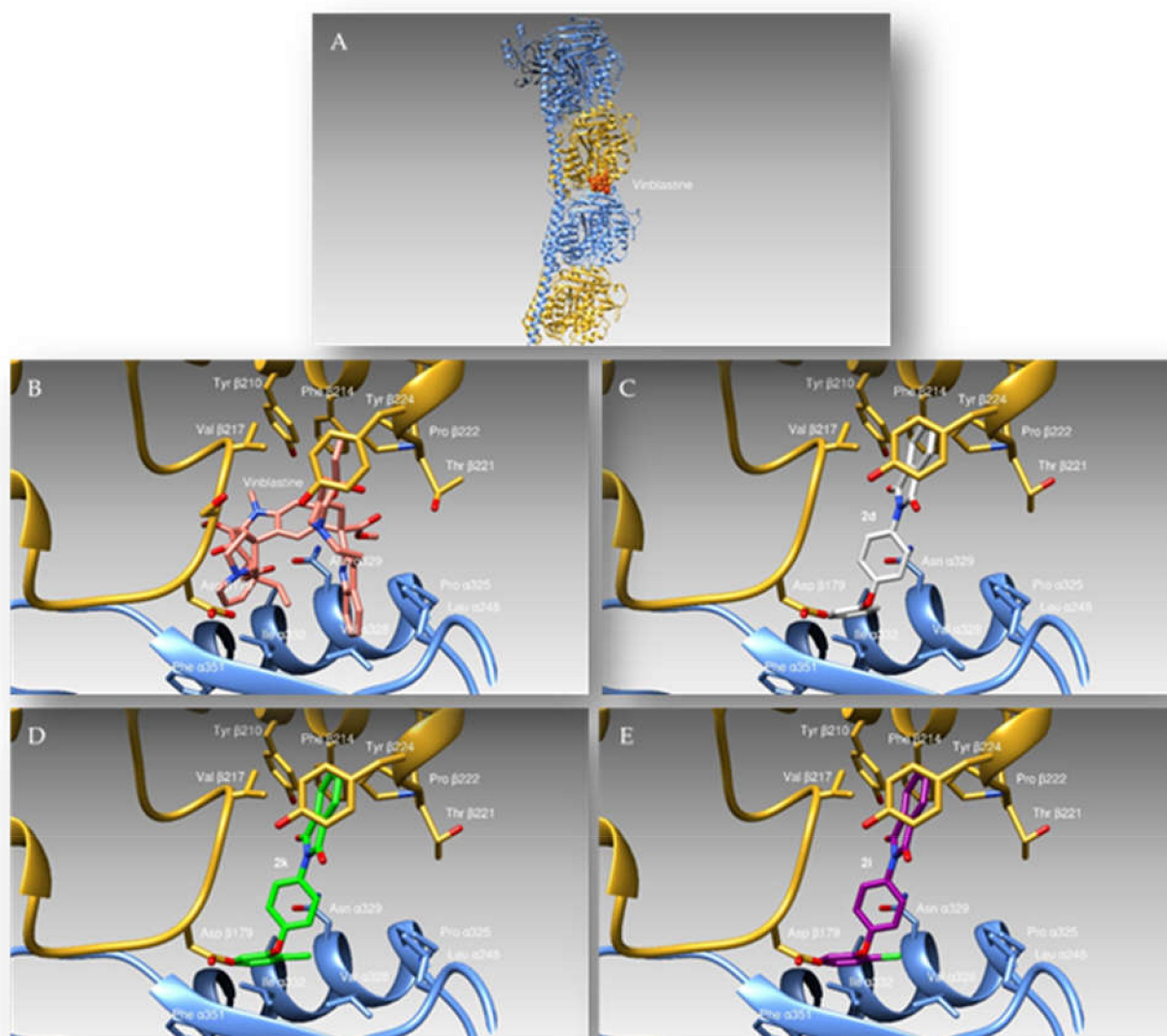


Figure 6. A schematic representation of the tetrameric $2\alpha 2\beta$ tubulin structure. α chain is reported as cyan ribbons, β as Golden ribbons (A). Compounds **2d**, **2k** and **2i** superpose to vinblastine binding site (B). (C–E) report the compounds **2d**, **2k** and **2i**, respectively, drawn as white, green and dark magenta sticks, bound to the vinblastine binding task of the protein.

4. Conclusions

Thalidomide, a drug well-known in the pharmaceutical history for its teratogenicity has been re-evaluated due to its antiangiogenic and immunomodulatory actions, which have made it effective against several malignancies. As a result, in the last decade, many researchers have concentrated their efforts on the design and development of new thalidomide analogs with improved efficacy and no or reduced toxicity. The focal point of our work was the synthesis and the biological evaluation of a series of thalidomide analogs (**2a–l**) for their potential anticancer activity toward a series of cell lines, including melanoma cells. Interestingly, compound **2k**, bearing a methyl group at the ortho position of the phenoxy moiety, exhibited a noteworthy cytotoxic effect against A2058 cells, thus becoming the most efficient compound of the series. A weak or no activity was detected for the other compounds. All the compounds under investigation have proven to be safe on the non-tumoral human embryonic renal cell line Hek-293. Furthermore, several studies agree on the importance of microtubule dynamics in governing the main cell functions, such as mitosis, maintaining of cell shape, cell division, intracellular transport, and chromosomes

segregation. Following this, we tested the ability of compound **2k** to target tubulin polymerization performing both an immunofluorescence assay in A2058 cells and an in vitro tubulin-polymerization assay. Data extrapolated from both the experiments evidenced that the compound **2k** interferes with the microtubule dynamics because of its capability of preventing tubulin polymerization. These interesting findings were also supported by docking studies that shown the ability of **2k** to superpose to vinblastine binding site in tubulin structure. Next, we performed a TUNEL assay proving that compound **2k** can induce the apoptotic process in A2058 melanoma cell line. To conclude, although most of the examined compounds did not display an encouraging activity, we aimed to focus our attention on a single compound (**2k**) from which we obtained auspicious results that make it a promising ally in the fight against cancer. However, further studies must be carried out to optimize this candidate and validate its efficacy in vivo.

Author Contributions: Conceptualization, M.S.S.; methodology, D.I. and A.C. (Alessia Carocci); software, C.R.; validation, C.F., formal analysis, A.B. and A.C. (Alessia Catalano); investigation, A.B. and A.C. (Alessia Catalano); data curation, D.I. and J.C.; writing—original draft preparation, A.C. (Alessia Carocci) and A.B.; supervision, M.S.S. and C.F. All authors have read and agreed to the published version of the manuscript.

Funding: The work of C.R. has been partially supported by a grant from the Italian Ministry of Health (Ricerca Corrente).

Institutional Review Board Statement: Not applicable.

Informed Consent Statement: Not applicable.

Conflicts of Interest: The authors declare no conflict of interest.

References

1. Sung, H.; Ferlay, J.; Siegel, R.L.; Laversanne, M.; Soerjomataram, I.; Jemal, A.; Bray, F. Global cancer statistics 2020: GLOBOCAN estimates of incidence and mortality worldwide for 36 cancers in 185 countries. *CA Cancer J. Clin.* **2021**, *71*, 209–249. [[CrossRef](#)]
2. Paolino, G.; Bekkenk, M.W.; Didona, D.; Eibenschutz, L.; Richetta, A.G.; Cantisani, C.; Viti, G.P.; Carbone, A.; Buccini, P.; De Simone, P.; et al. Is the prognosis and course of acral melanoma related to site-specific clinicopathological features? *Eur. Rev. Med. Pharmacol. Sci.* **2016**, *20*, 842–848. [[PubMed](#)]
3. Scali, E.; Mignogna, C.; Di Vito, A.; Presta, I.; Camastra, C.; Donato, G.; Bottoni, U. Inflammation and macrophage polarization in cutaneous melanoma: Histopathological and immunohistochemical study. *Int. J. Immunopathol. Pharmacol.* **2016**, *29*, 715–719. [[CrossRef](#)] [[PubMed](#)]
4. Chang, Q.; Long, J.; Hu, L.; Chen, Z.; Li, Q.; Hu, G. Drug repurposing and rediscovery: Design, synthesis, and preliminary biological evaluation of 1-arylamino-3-aryloxypropan-2-ols as anti-melanoma agents. *Bioorg. Med. Chem.* **2020**, *28*, 115404. [[CrossRef](#)] [[PubMed](#)]
5. Mercurio, A.; Adriani, G.; Catalano, A.; Carocci, A.; Rao, L.; Lentini, G.; Cavalluzzi, M.M.; Franchini, C.; Vacca, A.; Corbo, F. A mini-review on thalidomide: Chemistry, mechanisms of action, therapeutic potential and anti-angiogenic properties in multiple myeloma. *Curr. Med. Chem.* **2017**, *24*, 2736–2744. [[CrossRef](#)] [[PubMed](#)]
6. Zhang, S.; Li, M.; Gu, Y.; Liu, Z.; Xu, S.; Cui, Y.; Sun, B. Thalidomide influences growth and vasculogenic mimicry channel formation in melanoma. *J. Exp. Clin. Cancer Res.* **2008**, *27*, 1–9. [[CrossRef](#)]
7. Rashid, A.; Kuppa, A.; Kunwar, A.; Panda, D. Thalidomide (5HPP-33) suppresses microtubule dynamics and depolymerizes the microtubule network by binding at the vinblastine binding site on tubulin. *Biochemistry* **2015**, *54*, 2149–2159. [[CrossRef](#)]
8. Inatsuki, S.; Noguchi, T.; Miyachi, H.; Oda, S.; Iguchi, T.; Kizaki, M.; Hashimoto, Y.; Kobayashi, H. Tubulin-polymerization inhibitors derived from thalidomide. *Bioorg. Med. Chem. Lett.* **2005**, *15*, 321–325. [[CrossRef](#)]
9. Ghobrial, I.M.; Rajkumar, S.V. Management of thalidomide toxicity. *J. Support. Oncol.* **2003**, *1*, 194–205.
10. Pessoa, C.A.; Ferreira, P.M.P.; Lotufo, L.V.C.; de Moraes, M.O.; Cavalcanti, S.M.; Coêlho, L.C.D.; Hernandez, M.Z.; Leite, A.C.L.; De Simone, C.A.; Costa, V.M.; et al. Discovery of phthalimides as immunomodulatory and antitumor drug prototypes. *ChemMedChem Chem. Enabling Drug Discov.* **2010**, *5*, 523–528. [[CrossRef](#)]
11. Da Costa, P.M.; da Costa, M.P.; Carvalho, A.A.; Cavalcanti, S.M.T.; de Oliveira Cardoso, M.V.; de Oliveira Filho, G.B.; Viana, D.D.A.; Fechine-Jamacaru, F.V.; Leite, A.L.; De Moraes, M.O.; et al. Improvement of in vivo anticancer and antiangiogenic potential of thalidomide derivatives. *Chem. Biol. Interact.* **2015**, *239*, 174–183. [[CrossRef](#)]
12. Saturnino, C.; Caruso, A.; Longo, P.; Capasso, A.; Pingitore, A.; Cristina Caroleo, M.; Cione, E.; Perri, M.; Nicolo, F.; Mollica Nardo, V.; et al. Crystallographic study and biological evaluation of 1, 4-dimethyl-N-alkylcarbazoles. *Curr. Top. Med. Chem.* **2015**, *15*, 973–979. [[CrossRef](#)] [[PubMed](#)]

13. Ceramella, J.; Caruso, A.; Occhiuzzi, M.A.; Iacopetta, D.; Barbarossa, A.; Rizzuti, B.; Dallemagne, P.; Rault, S.; El-Kashef, H.; Saturnino, C.; et al. Benzothienquinazolinones as new multi-target scaffolds: Dual inhibition of human Topoisomerase I and tubulin polymerization. *Eur. J. Med. Chem.* **2019**, *181*, 111583. [[CrossRef](#)] [[PubMed](#)]
14. Sinicropi, M.S.; Iacopetta, D.; Rosano, C.; Randino, R.; Caruso, A.; Saturnino, C.; Muià, N.; Ceramella, J.; Puoci, F.; Rodriguez, M.; et al. N-thioalkylcarbazoles derivatives as new anti-proliferative agents: Synthesis, characterisation and molecular mechanism evaluation. *J. Enzym. Inhib. Med. Chem.* **2018**, *33*, 434–444. [[CrossRef](#)] [[PubMed](#)]
15. Ceramella, J.; Mariconda, A.; Rosano, C.; Iacopetta, D.; Caruso, A.; Longo, P.; Sinicropi, M.S.; Saturnino, C. α - ω Alkenyl-bis-S-Guanidine Thiourea Dihydrobromide Affects HeLa Cell Growth Hampering Tubulin Polymerization. *ChemMedChem* **2020**, *15*, 2306–2316. [[CrossRef](#)] [[PubMed](#)]
16. Iacopetta, D.; Lappano, R.; Mariconda, A.; Ceramella, J.; Sinicropi, M.S.; Saturnino, C.; Talia, M.; Cirillo, F.; Martinelli, F.; Puoci, F.; et al. Newly Synthesized Imino-Derivatives Analogues of Resveratrol Exert Inhibitory Effects in Breast Tumor Cells. *Int. J. Mol. Sci.* **2020**, *21*, 7797. [[CrossRef](#)]
17. Iacopetta, D.; Carocci, A.; Sinicropi, M.S.; Catalano, A.; Lentini, G.; Ceramella, J.; Curcio, R.; Caroleo, M.C. Old drug scaffold, new activity: Thalidomide-correlated compounds exert different effects on breast cancer cell growth and progression. *ChemMedChem* **2017**, *12*, 381–389. [[CrossRef](#)]
18. Aliabadi, A.; Gholamine, B.; Karimi, T. Synthesis and antiseizure evaluation of isoindoline-1,3-dione derivatives in mice. *Med. Chem. Res.* **2014**, *23*, 2736–2743. [[CrossRef](#)]
19. Assis, S.P.O.; Araújo, T.G.; Sena, V.L.; Catanho, M.T.J.; Ramos, M.N.; Srivastava, R.M.; Lima, V.L. Synthesis, hypolipidemic, and anti-inflammatory activities of arylphthalimides. *Med. Chem. Res.* **2014**, *23*, 708–716. [[CrossRef](#)]
20. Iacopetta, D.; Grande, F.; Caruso, A.; Mordocco, R.A.; Plutino, M.R.; Scrivano, L.; Ceramella, J.; Muià, N.; Saturnino, C.; Puoci, F.; et al. New insights for the use of quercetin analogs in cancer treatment. *Future Med. Chem.* **2017**, *9*, 2011–2028. [[CrossRef](#)]
21. Fazio, A.; Iacopetta, D.; La Torre, C.; Ceramella, J.; Muià, N.; Catalano, A.; Carocci, A.; Sinicropi, M.S. Finding solutions for agricultural wastes: Antioxidant and antitumor properties of pomegranate Akko peel extracts and β -glucan recovery. *Food Funct.* **2018**, *9*, 6618–6631. [[CrossRef](#)]
22. Ceramella, J.; Loizzo, M.R.; Iacopetta, D.; Bonesi, M.; Sicari, V.; Pellicanò, T.M.; Saturnino, C.; Malzert-Fréon, A.; Tundis, R.; Sinicropi, M.S. *Anchusa azurea* Mill. (Boraginaceae) aerial parts methanol extract interfering with cytoskeleton organization induces programmed cancer cells death. *Food Funct.* **2019**, *10*, 4280–4290. [[CrossRef](#)]
23. Iacopetta, D.; Rosano, C.; Sirignano, M.; Mariconda, A.; Ceramella, J.; Ponassi, M.; Saturnino, C.; Sinicropi, M.S.; Longo, P. Is the way to fight cancer paved with gold? Metal-based carbene complexes with multiple and fascinating biological features. *Pharmaceuticals* **2020**, *13*, 91. [[CrossRef](#)]
24. Tundis, R.; Iacopetta, D.; Sinicropi, M.S.; Bonesi, M.; Leporini, M.; Passalacqua, N.G.; Ceramella, J.; Menichini, F.; Loizzo, M. Assessment of antioxidant, antitumor and pro-apoptotic effects of *Salvia fruticosa* Mill. subsp. *thomasii* (Lacaita) Brullo, Guglielmo, Pavone & Terrasi (Lamiaceae). *Food Chem. Toxicol.* **2017**, *106*, 155–164.
25. Rechoum, Y.; Rovito, D.; Iacopetta, D.; Barone, I.; Andò, S.; Weigel, N.L.; O'Malley, B.W.; Brown, P.H.; Fuqua, S.A.W. AR collaborates with ER α in aromatase inhibitor-resistant breast cancer. *Breast Cancer Res. Treat.* **2014**, *147*, 473–485. [[CrossRef](#)]
26. Waight, A.B.; Bargsten, K.; Doronina, S.; Steinmetz, M.O.; Sussman, D.; Prota, A.E. Structural Basis of Microtubule Destabilization by Potent Auristatin Anti-Mitotics. *PLoS ONE* **2016**, *11*, e0160890. [[CrossRef](#)]
27. Morris, G.M.; Huey, R.; Lindstrom, W.; Sanner, M.F.; Belew, R.K.; Goodsell, D.S.; Olson, A.J. Autodock4 and AutoDockTools4: Automated docking with selective receptor flexibility. *J. Comput. Chem.* **2009**, *30*, 2785–2791. [[CrossRef](#)]
28. Sanner, M.F.; Duncan, B.S.; Carrillo, C.J.; Olson, A.J. Integrating computation and visualization for biomolecular analysis: An example using python and AVS. *Pac. Symp. Biocomput.* **1999**, *8*, 401–412.
29. Cesarini, S.; Spallarossa, A.; Ranise, A.; Schenone, S.; Rosano, C.; La Colla, P.; Sanna, G.; Busonera, B.; Loddo, R. N-acylated and N,N'-diacylated imidazolidine-2-thione derivatives and N,N'-diacylated tetrahydropyrimidine-2(1H)-thione analogues: Synthesis and antiproliferative activity. *Eur. J. Med. Chem.* **2009**, *44*, 1106–1118. [[CrossRef](#)]
30. Viale, M.; Cordazzo, C.; de Totero, D.; Budriesi, R.; Rosano, C.; Leoni, A.; Ioan, P.; Aiello, C.; Croce, M.; Andreani, A.; et al. Inhibition of MDR1 activity and induction of apoptosis by analogues of nifedipine and diltiazem: An in vitro analysis. *Investig. New Drugs* **2011**, *29*, 98–109. [[CrossRef](#)]
31. Rosano, C.; Lappano, R.; Santolla, M.F.; Ponassi, M.; Donadini, A.; Maggolini, M. Recent advances in the rationale design of GPER ligands. *Curr. Med. Chem.* **2012**, *19*, 6199–6206. [[CrossRef](#)]
32. Saturnino, C.; Iacopetta, D.; Sinicropi, M.S.; Rosano, C.; Caruso, A.; Caporale, A.; Marra, N.; Marengo, B.; Pronzato, M.A.; Parisi, O.I.; et al. N-alkyl carbazole derivatives as new tools for Alzheimer's disease: Preliminary studies. *Molecules* **2014**, *19*, 9307–9317. [[CrossRef](#)]
33. Pettersen, E.F.; Goddard, T.D.; Huang, C.C.; Couch, G.S.; Greenblatt, D.M.; Meng, E.C.; Ferrin, T.E. UCSF Chimera- A visualization system for exploratory research and analysis. *J. Comput. Chem.* **2004**, *25*, 1605–1612. [[CrossRef](#)]
34. Brouhard, G.J.; Rice, L.M. Microtubule dynamics: An interplay of biochemistry and mechanics. *Nat. Rev. Mol. Cell Biol.* **2018**, *19*, 451–463. [[CrossRef](#)]
35. Zhang, D.; Kanakkanthara, A. Beyond the paclitaxel and Vinca alkaloids: Next generation of plant-derived microtubule-targeting agents with potential anticancer activity. *Cancers* **2020**, *12*, 1721. [[CrossRef](#)] [[PubMed](#)]

36. Dumontet, C.; Jordan, M.A. Microtubule-binding agents: A dynamic field of cancer therapeutics. *Nat. Rev. Drug Discov.* **2010**, *9*, 790–803. [[CrossRef](#)]
37. Yele, V.; Pindiprolu, S.K.S.; Sana, S.; Ramamurty, D.S.V.N.M.; Madasi, J.R.; Vadlamani, S. Synthesis and preclinical evaluation of indole triazole conjugates as microtubule targeting agents that are effective against MCF-7 breast cancer cell lines. *Anti-Cancer Agents Med. Chem.* **2021**, *21*, 1047–1055. [[CrossRef](#)]
38. Karahalil, B.; Yardim-Akaydin, S.; Nacak Baytas, S. An overview of microtubule targeting agents for cancer therapy. *Arch. Hyg. Rada Toksikol.* **2019**, *70*, 160–172. [[CrossRef](#)]
39. Kaur, R.; Kaur, G.; Gill, R.K.; Soni, R.; Bariwal, J. Recent developments in tubulin polymerization inhibitors: An overview. *Eur. J. Med. Chem.* **2014**, *87*, 89–124. [[CrossRef](#)]
40. Liu, J.; Xue, D.; Zhu, X.; Yu, L.; Mao, M.; Liu, Y. Anticancer evaluation of a novel dithiocarbamate hybrid as the tubulin polymerization inhibitor. *Investig. New Drugs* **2020**, *38*, 525–532. [[CrossRef](#)]
41. Donthiboina, K.; Anchi, P.; Ramya, P.S.; Karri, S.; Srinivasulu, G.; Godugu, C.; Shankaraiah, N.; Kamal, A. Synthesis of substituted biphenyl methylene indolinones as apoptosis inducers and tubulin polymerization inhibitors. *Bioorg. Chem.* **2019**, *86*, 210–223. [[CrossRef](#)] [[PubMed](#)]
42. Iacopetta, D.; Catalano, A.; Ceramella, J.; Barbarossa, A.; Carocci, A.; Fazio, A.; La Torre, C.; Caruso, A.; Ponassi, M.; Rosano, C.; et al. Synthesis, anticancer and antioxidant properties of new indole and pyranoindole derivatives. *Bioorg. Chem.* **2020**, *105*, 104440. [[CrossRef](#)]
43. Elmore, S. Apoptosis: A review of programmed cell death. *Toxicol. Pathol.* **2007**, *35*, 495–516. [[CrossRef](#)] [[PubMed](#)]
44. Almahli, H.; Hadchity, E.; Jaballah, M.Y.; Daher, R.; Ghabbour, H.A.; Kabil, M.M.; Al-Shakliah, N.S.; Eldehna, W.M. Development of novel synthesized phthalazinone-based PARP-1 inhibitors with apoptosis inducing mechanism in lung cancer. *Bioorg. Chem.* **2018**, *77*, 443–456. [[CrossRef](#)]
45. Chaitanya, G.V.; Alexander, J.S.; Babu, P.P. PARP-1 cleavage fragments: Signatures of cell-death proteases in neurodegeneration. *Cell. Commun. Signal* **2010**, *8*, 1–11. [[CrossRef](#)] [[PubMed](#)]
46. Lappano, R.; Rosano, C.; Pisano, A.; Santolla, M.F.; De Francesco, E.M.; De Marco, P.; Dolce, V.; Ponassi, M.; Felli, L.; Cafeo, G.; et al. Calixpyrrole derivative acts as an antagonist to GPER, a G-protein coupled receptor: Mechanisms and models. *Dis. Model. Mech.* **2015**, *8*, 1237–1246. [[CrossRef](#)]
47. Sinicropi, M.S.; Lappano, R.; Caruso, A.; Santolla, M.F.; Pisano, A.; Rosano, C.; Capasso, A.; Panno, A.; Lancelot, J.C.; Rault, S.; et al. (6-bromo-1,4-dimethyl-9H-carbazol-3-yl-methylene)-hydrazine (carbhydraz) acts as a GPER agonist in breast cancer cells. *Curr. Top. Med. Chem.* **2015**, *15*, 1035–1042. [[CrossRef](#)] [[PubMed](#)]
48. Stec-Martyna, E.; Ponassi, M.; Miele, M.; Parodi, S.; Felli, L.; Rosano, C. Structural comparison of the interaction of tubulin with various ligands affecting microtubule dynamics. *Curr. Cancer Drug Targets* **2012**, *12*, 658–666. [[CrossRef](#)]